

Effect of processing parameter on wear resistance property of laser material deposited titanium-alloy composite

R. M. MAHAMOOD^{a,b}, E. T. AKINLABI^a

^a*Department of Mechanical Engineering Science, University of Johannesburg, Auckland Park Kingsway Campus, Johannesburg, 2006, South Africa.*

^b*Department of Mechanical Engineering, University of Ilorin, Nigeria*

An empirical model was developed for predicting the wear resistance behaviour of laser metal deposited TiC/Ti6Al4V composite. The influence of the processing parameters, laser power, scanning speed, powder flow rate and gas flow rate, on the wear resistance property of the deposited samples were extensively studied. The experiment was designed and analyzed using a two level full factorial Design of Experiment using Design Expert 9 statistical software. The laser power was set between 1.8 and 3.2 kW, the scanning speed between 0.002 and 0.006 m/s, the powder flow rate between was set between 2 and 4 g/min and the gas flow rate was set between 2 and 4 l/min. These settings were chosen based on the trial experiments performed to establish process window after depositing pore free TiC/Ti6Al4V composites. Six (6) tracks with 50% overlap percentage each were produced at processing parameters generated from the Design Expert software. The deposition process was produced using a 4.0 kW Nd: YAG laser. The wear test was carried out using UMT 2CETR tribotester with ball-on-plate arrangement under dry condition. Detailed statistical analysis was studied and the developed model was validated by performing additional experiment at processing parameters that are different from the ones used to develop the model. The model was found to be in good agreement with the experimental data and the model can be used to navigate the design space

Received September 9, 2014; accepted September 9, 2015)

Keywords: Additive Manufacturing; Design of Experiment; Full factorial design; Laser-Metal Deposition; Microstructure; Titanium Alloy Composite; Wear Resistance

1. Introduction

Titanium and its alloys are widely used in aerospace, chemical, petrochemical, marine and medical applications because the exciting properties they possess such as high strength-to-weight ratio, low density, excellent corrosion resistance, high Young's modulus and they also maintain most of these properties at high temperature [1]. Ti6Al4V is the most widely used Titanium alloy and it is often referred to as the workhorse of the industry [2]. In spite of these excellent properties, it has a poor wear resistance property [3,4] which has restricted its application in areas where it will be exposed to come in contact with self or other materials especially in sliding motion [5]. Therefore, it is imperative to improve the wear resistance property of Titanium and its alloy where it will be used in applications requiring this property.

A number of surface modifications have been reported in the literature to improve the wear-resistance behaviour of titanium and its alloys. These include the conventional chemical heat treatment, such as surface boriding [6], surface carburizing [7], and surface nitriding [8]. Some of the disadvantages of these surface modification techniques include long processing time and easy deformation of the material being treated [9]. Thermal spray coating is another form of surface modification. The thermal

spraying technique is limited by bonding strength [9]. Laser surface modification is the most popular type of surface modification technique that is used for titanium and its alloys [10]. The laser surface modification uses the advantage of coherent nature of the laser beam, which can be easily controlled and focused only on the needed area. Some of the laser-surface modification techniques include laser surface heating and melting, laser surface alloying and laser material deposition [11]. Laser surface re-melting has been applied to improve the wear-resistance performance of Ti6Al4V in the literature [12, 13]. In laser re-melting, the surface of the material is re-melted, so that the solidification process can be controlled to achieve a controlled grain structure. Rapid cooling, for example, would result in a martensitic microstructure, which is very hard and brittle. Laser surface alloying has also been applied to modify the wear behaviour of Ti6Al4V. These include: laser gas alloying [14] and laser powder alloying [15]. The laser alloying is achieved by melting the surface and the alloying materials (gas or powder) to improve the surface properties of the material. Laser surface alloying has been reported to be a promising technique in the literature due to some benefits it provides [16-19]. One of the disadvantages of laser surface alloying is that, it creates thermal distortions in the bulk material that produces severe residual stresses because of large heat

affected zone. Another surface modification that is performed on titanium and its alloys is addition of composite materials coated on the surface of Ti6Al4V using laser deposition process, [20, 24] in order to improve its wear-resistance performance. Improving the wear resistance properties of titanium through laser material deposition for wear resistant coating is more beneficial because of the low heat affected zone produced during this process.

Laser material deposition (LMD) process also known as laser metal deposition process is an advanced manufacturing process that belongs to the Directed Energy Deposition (DED) class of additive manufacturing (AM) technology [25]. LMD can be used to produce functional parts directly from the three dimensional (3D) computer aided design (CAD) model of the part being produced, simply by adding material layer after layer until the part is finished [26]. LMD is an important AM technology that is capable of repairing high valued component parts which were prohibitive in the past [27]. LMD can use multi materials simultaneously making it possible to produce part that is made up of composite material as well as functionally graded material in a single manufacturing run [28]. Despite the exciting properties of the technology, there is still much to be understood about the material characterization of parts produced from this process. A number of studies have appeared in the literature to relate the effect of processing parameters on the properties of the material produced through this process [20, 21, 24, and 29].

In this study, the influence of processing parameters on wear resistance property of laser deposited TiC/Ti6Al4V composite was studied. TiC/Ti6Al4V composite found its applications in aerospace and medical use to mention but a few due to its excellent mechanical properties and bio-compatibility [30]. Full factorial design of experiment was used to design as well as analyze the results obtained. This is to enable statistical inference to be drawn on the results obtained. An empirical model was developed and validated. The results are extensively analyzed and presented.

2. Experimental Methods

An annealed 5mm thick 99.6% pure Ti6Al4V sheet was used as substrate for the laser deposition of the TiC/Ti6Al4V composite samples. The sheet was supplied by VSMPO-AVISMA Corporation, Russia. This alloy contains approximately 6 w% of Aluminum, which is an alpha-stabilizing element and approximately 4 w% of Vanadium, a beta-phase stabilizing element. The sheet was cut into square shape of 72 x 72 mm. The substrates were sandblasted and cleaned with acetone before the deposition process. The purpose of sandblasting the

surface of substrate was to aid the laser-power absorption process, because a shining surface would reflect most of the laser beam. The Ti6Al4V powder use is also 99.6% pure and with particle size of between 120 and 350 μm . It is a spherically shaped gas-atomized powder. The TiC powder used in this study is a ball-milled powder of particle size range below 60 μm . The Ti6Al4V and the TiC powder were supplied by F.J. Brodmann and Co., L.L.C., Louisiana. A 4.0 kW Nd: YAG laser attached to a Kuka robot was used to achieve laser material deposition process. The spot diameter was maintained at 2mm at a focal distance of 195mm above the substrate. A co-axial nozzle was attached to the robot's end effector for powder delivery. Argon gas was used for carrying the powder as well as to provide shield for the deposited samples. The experimental set-up is shown in Figure 1.

Trial experiments were performed in order to establish the process window for the deposition of the porous free and fully dense deposit of TiC/Ti6Al4V. The results from these trial runs formed the basis for the selection of the lower levels selected for the design of experiment. The laser power, scanning speed, powder flow rate and powder flow rate were set at lower levels and higher levels for the full factorial design as presented in Table 1. This information was entered into the Design Expert software with one replicate and the Experimental matrix was generated. A total of thirty two experiments were conducted. Six tracks of 50 w % TiC were deposited at 50% overlap.

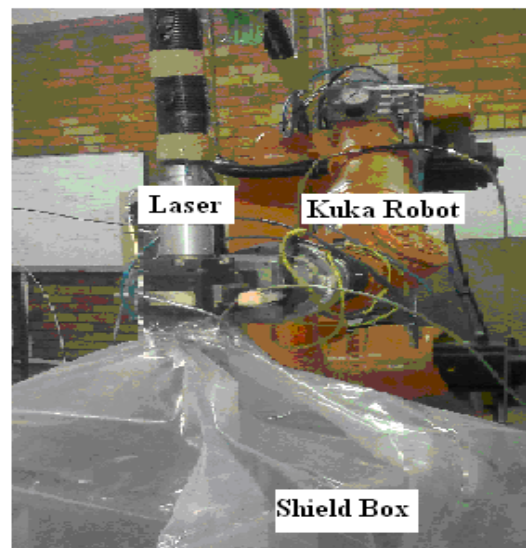


Fig. 1. Experimental set-up [31]

Table 1. Coded values of the lower and higher levels of the processing parameters

Factor	Name	Units	Minimum	Maximum	Coded Values		Mean	SD
A	Laser power	kW	1.80	3.20	- 1.000 =1.80	1.000 =3.20	2.50	0.70
B	Scanning Speed	m/s	0.002	0.006	-1.000 =0.002	1.000 =0.006	0.004	0.002
C	Powder Flow Rate	g/min	2.00	4.00	-1.000 =2.00	1.000 =4.00	3.00	1.00
D	Gas Flow Rate	l/min	2.00	4.00	-1.000 =2.00	1.000=4.00	3.00	1.00

The metallographic samples were cut across the deposition direction and mounted in hot resin. The mounted samples were ground, and polished according to the standard metallographic sample preparation for Titanium and its alloys. The samples were etched using Kroll's reagent. The microstructure was characterized using TESCAN Scanning Electron Microscopy (SEM). The wear-resistance test was performed using a universal material tester UMT 2CETR tribotester with ball-on-plate arrangement under dry condition (no lubrication). The ball is a tungsten carbide sphere with a diameter of 10 mm, at a load of 25 N, stroke length of 2mm, and a reciprocating frequency of 20 Hz and for 1200s. The coefficient of friction was measured for all the samples and recorded. The wear test was performed, according to ASTM G133 - 05(2010) Standard (ASTM G133, 2010). The wear surface was analyzed using the SEM. The wear volumes were determined from information obtained from the wear-track surface profile, that is, the cross-section of a wear track. A micrograph of a wear track showing the wear diameter and the stroke length is shown in Fig. 2.

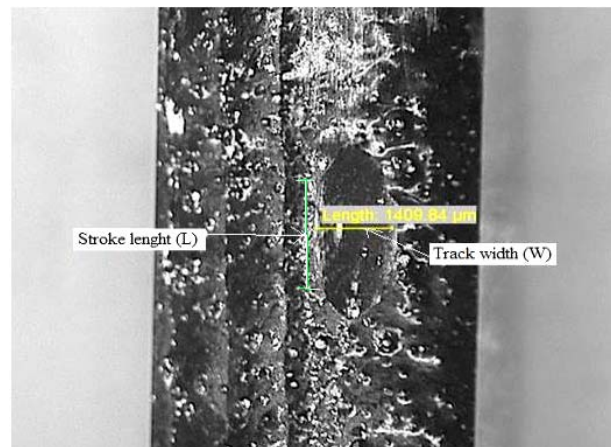


Fig. 2. Micrograph of a wear track showing the wear-track width and the stroke length

Then the wear volume loss was obtained by using the formula proposed by Sharma et al. (2013) [32] in eq. 1.

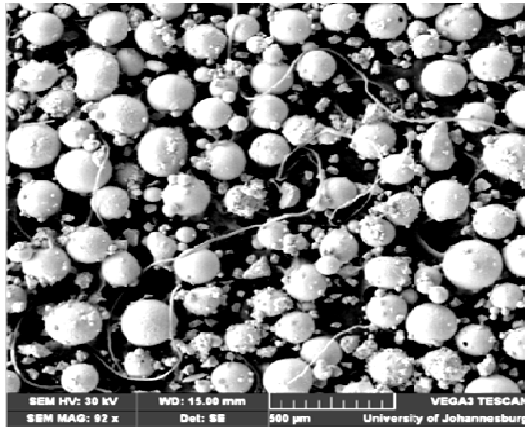
$$V = L \left[r^2 \sin^{-1} \left(\frac{w}{2r} \right) - \frac{w}{2} \left(r^2 - \frac{w^2}{4} \right)^{1/2} \right] + \frac{\pi}{3} \left[2r^3 - 2r^2 \left(r^2 - \frac{w^2}{4} \right)^{1/2} - \frac{w^2}{4} \left(r^2 - \frac{w^2}{4} \right)^{1/2} \right] \quad (1)$$

Where v is the wear volume in mm^3 , r is the ball radius, w and L are the wear-track width and the stroke length, respectively (see Fig. 2). The wear volume was calculated by using equation 1.

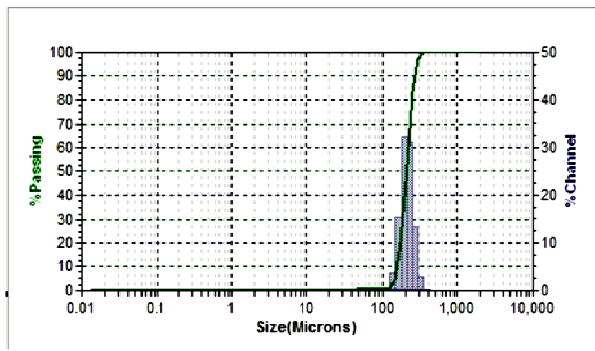
3. Results

The morphology of the Ti6Al4V powder is shown in Figure 3a. The particle size analysis of the Ti6Al4V powder is shown in Fig. 3b.

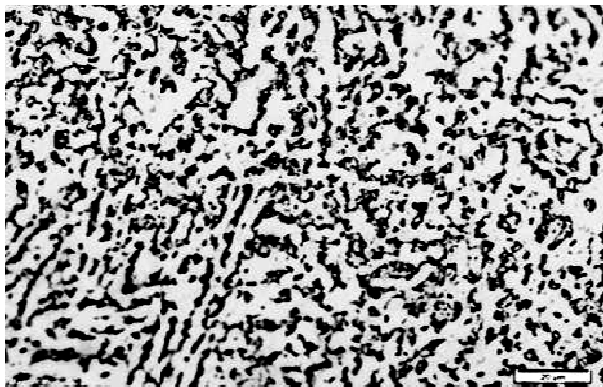
The micrograph of the Ti6Al4V substrate is shown in Fig. 3c. The Ti6Al4V powder is characterized by a spherical shape and smooth surfaces. Atomized powders are mostly preferred in laser deposition process because they exhibit low surface oxidation due to the reduced total surface area.



(a)



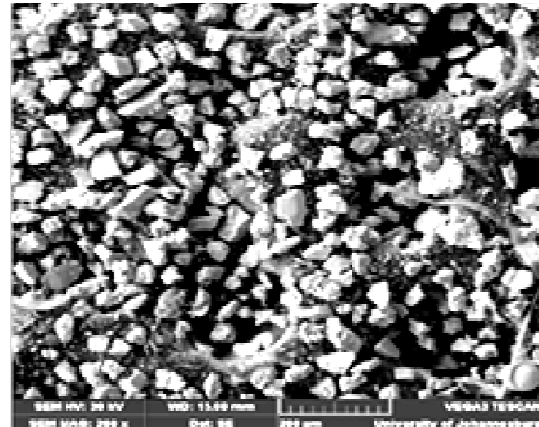
(b)



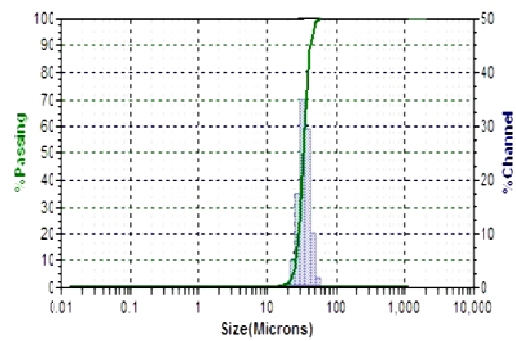
(c)

Fig. 3(a) SEM micrograph showing the morphology of the Ti6Al4V powder [29] (b) Particle size analysis of Ti6Al4V powder; (c) the micrograph of the substrate

The morphology of the TiC powder is shown in Fig. 4a and the particle size analysis is shown in Fig. 4b. The TiC powder is characterized by irregular shape which is typical of a ball milled powder. The photograph of some of the deposited samples is shown in Fig. 5.



(a)



(b)

Fig. 4: (a) SEM micrograph of TiC powder [33] (b) Particle size analysis of TiC powder



Fig. 5. Photograph of some of the samples after the deposition process

The stroke length used in this study is 2mm; and the diameter of the Tungsten Carbide ball was 10mm. Microsoft Excel was used to generate the wear-volume loss results. The full-factorial design with the wear-volume loss results is presented in Table 2.

Table 2: Results of the coded Full-factorial design

Std.	Run	Factor 1 A:Laser Power (kW)	Factor 2 B:Scanning Speed (m/s)	Factor 3 C:Powder Flow Rate (g/min)	Factor 4 D:Gas Flow Rate (l/min)	Response 1 wear volume (mm ³)
25	1	-1	-1	1	1	0.0446
11	2	1	-1	1	-1	0.1072
24	3	1	1	-1	1	0.1023
17	4	-1	-1	-1	1	0.0442
20	5	1	-1	-1	1	0.1388
15	6	1	1	1	-1	0.0753
23	7	1	1	-1	1	0.1003
28	8	1	-1	1	1	0.1101
9	9	-1	-1	1	-1	0.0175
4	10	1	-1	-1	-1	0.1631
22	11	-1	1	-1	1	0.0211
3	12	1	-1	-1	-1	0.1611
6	13	-1	1	-1	-1	0.015
30	14	-1	1	1	1	0.0162
27	15	1	-1	1	1	0.1167
2	16	-1	-1	-1	-1	0.0308
18	17	-1	-1	-1	1	0.0398
5	18	-1	1	-1	-1	0.0119
21	19	-1	1	-1	1	0.0213
7	20	1	1	-1	-1	0.0681
8	21	1	1	-1	-1	0.0667
1	22	-1	-1	-1	-1	0.0316
12	23	1	-1	1	-1	0.1074
10	24	-1	-1	1	-1	0.0187
14	25	-1	1	1	-1	0.0512
32	26	1	1	1	1	0.0252
31	27	1	1	1	1	0.0232
26	28	-1	-1	1	1	0.0456
29	29	-1	1	1	1	0.0162
19	30	1	-1	-1	1	0.1394
13	31	-1	1	1	-1	0.0532
16	32	1	1	1	-1	0.0773

The full-factorial design was analysed in the Design expert 9 software. The results are analysed numerically and graphically.

Numerical Analysis

The design matrix evaluation for the chosen factorial Model is presented in Table 3. A minimum of 3 lack of fit degree of freedom and 4 degree of freedom for pure error is recommended to ensure a valid lack of fit test. From the Table, the 4 lack of fit degree of freedom and the 16 for the pure error are good to detect lack of fit. There were no aliases found for this Model. The analysis of variance of the selected model is presented in Table 4.

Table 3. Degrees of Freedom for Evaluation

Model	11
Residuals	20
Lack of Fit	4
Pure Error	16
Corr. Total	31

From Table 4, the Model F-value of 1070.56 implies that the model is significant and that there is only a 0.01% chance that an F-value this large could occur due to noise. Values of "Prob > F" less than 0.0500 indicates that the

model terms are significant. In this case A, B, C, D, AB, AC, AD, BC, BD, CD, ABC, ABD, ACD, BCD, ABCD are significant model terms. The R-square analysis is presented in Table 5.

Table 4. Analysis of variance (ANOVA) for the selected factorial model

Source	Sum of Squares	df	Mean Square	F Value	p-value Prob > F	
Model	0.26	15	0.017	1070.56	< 0.0001	significant
A-Laser Power	0.15	1	0.15	9388.09	< 0.0001	
B-Scanning Speed	0.037	1	0.037	2258.49	< 0.0001	
C-Powder Flow Rate	4.885E-003	1	4.885E-003	301.04	< 0.0001	
D-Gas Flow Rate	2.858E-004	1	2.858E-004	17.61	0.0007	
AB	0.013	1	0.013	783.68	< 0.0001	
AC	0.013	1	0.013	774.89	< 0.0001	
AD	1.719E-003	1	1.719E-003	105.91	< 0.0001	
BC	1.108E-003	1	1.108E-003	68.26	< 0.0001	
BD	5.993E-003	1	5.993E-003	369.32	< 0.0001	
CD	6.157E-003	1	6.157E-003	379.44	< 0.0001	
ABC	3.355E-003	1	3.355E-003	206.72	< 0.0001	
ABD	2.309E-003	1	2.309E-003	142.32	< 0.0001	
ACD	4.374E-004	1	4.374E-004	26.95	< 0.0001	
BCD	0.020	1	0.020	1224.85	< 0.0001	
ABCD	1.761E-004	1	1.761E-004	10.85	0.0046	
Pure Error	2.596E-004	16	1.623E-005			
Cor Total	0.26	31				

Table 5. R-Squared analysis

Std. Dev.	4.028E-003	R-Squared	0.9990
Mean	0.24	Adj. R-Squared	0.9981
C.V. %	1.70	Pred. R-Squared	0.9960
PRESS	1.039E-003	Adeq. Precision	100.697

The "Pred. R-Squared" of 0.9960 is in reasonable agreement with the "Adj. R-Squared" of 0.9981 because the difference is less than 0.2. "Adeq. Precision" measures the signal to noise ratio. A ratio greater than 4 is desirable. In this case ratio of 100.697 indicates an adequate signal and this model can be used to navigate the design space. The analysis of the model terms are presented in Table 6.

Table 6. Model terms analysis

Factor	Coefficient Estimate	df	Standard Error	95% CI Low	95% CI High	VIF
Intercept	0.24	1	7.121E-004	0.24	0.24	
A-Laser Power	0.069	1	7.121E-004	0.067	0.071	1.00
B-Scanning Speed	-0.034	1	7.121E-004	-0.035	-0.032	1.00
C-Powder Flow Rate	-0.012	1	7.121E-004	-0.014	-0.011	1.00
D-Gas Flow Rate	-2.988E-003	1	7.121E-004	-4.498E-003	-1.479E-003	1.00
AB	-0.020	1	7.121E-004	-0.021	-0.018	1.00
AC	-0.020	1	7.121E-004	-0.021	-0.018	1.00
AD	-7.328E-003	1	7.121E-004	-8.838E-003	-5.819E-003	1.00
BC	5.884E-003	1	7.121E-004	4.374E-003	7.393E-003	1.00
BD	-0.014	1	7.121E-004	-0.015	-0.012	1.00

Factor	Coefficient Estimate	df	Standard Error	95% CI Low	95% CI High	VIF
CD	-0.014	1	7.121E-004	-0.015	-0.012	1.00
ABC	-0.010	1	7.121E-004	-0.012	-8.729E-003	1.00
ABD	8.495E-003	1	7.121E-004	6.986E-003	0.010	1.00
ACD	-3.697E-003	1	7.121E-004	-5.207E-003	-2.188E-003	1.00
BCD	-0.025	1	7.121E-004	-0.026	-0.023	1.00
ABCD	-2.346E-003	1	7.121E-004	-3.856E-003	-8.364E-004	1.00

The final Equation in Terms of Coded Factors is given in equation 2

$$\begin{aligned}
 \text{Sqrt (wear volume)} = & +0.24 \\
 & +0.069 * A \\
 & -0.034 * B \\
 & -0.012 * C \\
 & -2.988E-003 * D \\
 & -0.020 * AB \\
 & -0.020 * AC \\
 & -7.328E-003 * AD \\
 & +5.884E-003 * BC \\
 & -0.014 * BD \\
 & -0.014 * CD \\
 & -0.010 * ABC \\
 & +8.495E-003 * ABD \\
 & -3.697E-003 * ACD \\
 & -0.025 * BCD \\
 & -2.346E-003 * ABCD
 \end{aligned}
 \tag{2}$$

The equation 2 can be used to make predictions about the response for given levels of each factor. The high levels of the factors are coded as +1 and the low levels of the factors are coded as -1. The coded equation is useful for identifying the relative impact of the factors by comparing the factor coefficients. The Final Equation in Terms of Actual Factors is given in Equation 3

$$\begin{aligned}
 \text{Sqrt(wear volume)} = & +0.23719 \\
 & +0.068999 * \text{Laser Power} \\
 & -0.033843 * \text{Scanning Speed} \\
 & -0.012356 * \text{Powder Flow Rate} \\
 & -2.98831E-003 * \text{Gas Flow Rate} \\
 & -0.019935 * \text{Laser Power} * \text{Scanning Speed} \\
 & -0.019823 * \text{Laser Power} * \text{Powder Flow Rate} \\
 & -7.32845E-003 * \text{Laser Power} * \text{Gas Flow Rate}
 \end{aligned}$$

$$\begin{aligned}
 & +5.88358E-003 * \text{Scanning Speed} * \text{Powder Flow Rate} \\
 & -0.013685 * \text{Scanning Speed} * \text{Gas Flow Rate} \\
 & -0.013872 * \text{Powder Flow Rate} * \text{Gas Flow Rate} \\
 & -0.010239 * \text{Laser Power} * \text{Scanning Speed} * \\
 & \quad \text{Powder Flow Rate} \\
 & +8.49536E-003 * \text{Laser Power} * \text{Scanning Speed} * \text{Gas} \\
 & \quad \text{Flow Rate} \\
 & -3.69713E-003 * \text{Laser Power} * \text{Powder Flow Rate} * \text{Gas} \\
 & \quad \text{Flow Rate} \\
 & -0.024923 * \text{Scanning Speed} * \text{Powder Flow Rate} * \\
 & \quad \text{Gas Flow Rate} \\
 & -2.34599E-003 * \text{Laser Power} * \text{Scanning Speed} * \\
 & \quad \text{Powder Flow Rate} * \text{Gas Flow Rate}
 \end{aligned}
 \tag{3}$$

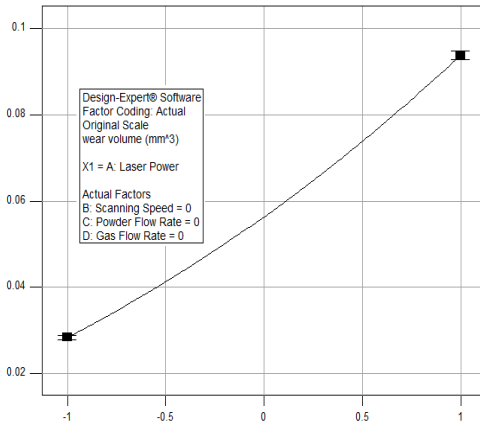
The equation 3 can be used to make predictions about the response for given levels of each factor.

Graphical analysis

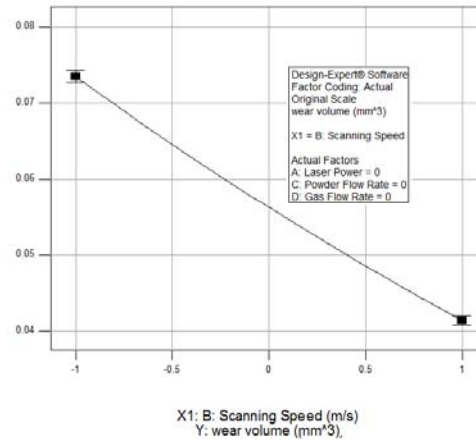
The main effect plot of laser power, scanning speed, powder flow rate and gas flow rate is shown in Figure 6a, 6b, 6c and 6d respectively. The main effect plot of the laser power, as shown in Figure 6a, indicates that the laser power has a very strong effect on the wear-volume loss. This is because the graph has a positive slope. The laser power has a positive effect on the wear-volume loss; as the laser power was increased, the wear-volume loss was also increased. This is because at very high laser power more of the TiC powder are melted thereby resulting in the presence of few unmelted carbide particles. Unmelted carbide particles are found to be responsible for improved wear resistance performance due to the lubricating effect they produce during slidding actions [24]. The scanning speed on the other hand has a negative effect on the wear-volume loss, as shown in Figure 6b, because it has a negative slope. The wear-volume loss was found to decrease, as the scanning speed was increased. At low scanning, the wear volume loss is very high because the laser material interaction time is high thereby resulting in fewer unmelted carbide particles. Whereas at high scanning speed, the laser material interaction time is less and there are more unmelted carbide particles present which improves the wear resistance and hence low wear volume loss. A similar response was observed in Figure 6c, for the powder flow rate. Although, the slope is less steepy

when compared with that of the scanning speed in Figure 6b. When the powder flow rate is high, the wear volume loss is low because more powder delivery into the melt pool results in the presence of more unmelted carbide. The least-significant factor is the gas flow rate, which is shown in Fig. 6d. The is least steeply when compared to

the powder flow rate and the scanning speed. Gas flow rate has little effect on wear volume loss, high gas flow rate results in slight decrease in wear volume loss. This is as a result of its contribution to the stirring effect it has on the melt pool by helping to disperse the TiC powder which helps to improve wear resistance.

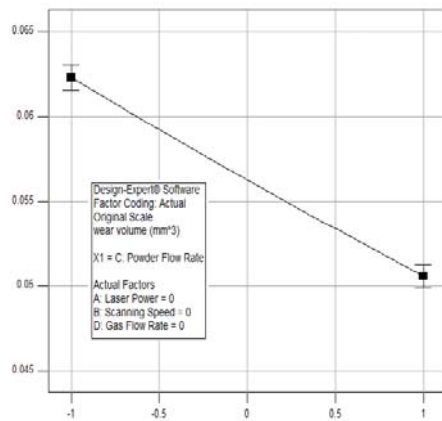


X1: A: Laser Power (kW)
Y: wear volume (mm³)
(a)



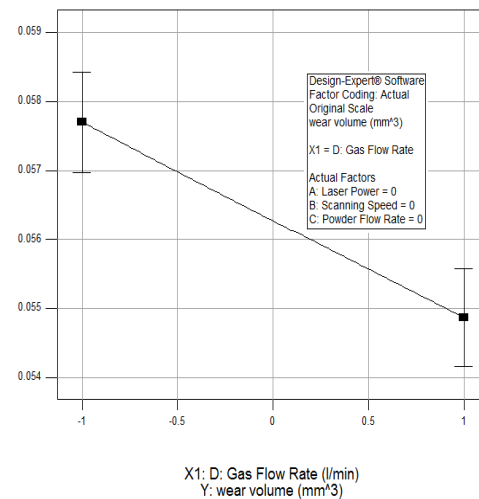
X1: B: Scanning Speed (m/s)
Y: wear volume (mm³)

(b)



X1: C: Powder Flow Rate (g/min)
Y: wear volume (mm³)

(c)



X1: D: Gas Flow Rate (l/min)
Y: wear volume (mm³)

(d)

Fig. 6: Main effect plot of: (a) laser power; (b) scanning speed; (c) powder flow rate; and (d) gas flow rate

The interaction plots between the laser power and scanning speed and powder-flow rate are shown in Figure 7. An interaction is observed when the response of one factor is dependent on the level of the other factor. That is, a different response is observed when one factor is fixed at a level, and the level of the other factor is changed. An interaction can be identified when the lines of the two graphs are not parallel.

If the imaginary angle between the lines is large, this implies that there is a strong interaction between the two factors. A stronger interaction was observed between the laser power and the scanning speed (see Fig. 7a) when compared with the interaction between the laser power and

the powder flow rate (see Figure 7b). The interaction between the laser power and the gas flow rate is shown in Fig. 7c while the interaction between the powder flow rate and scanning speed are shown in Figure 7d. The interaction between the laser power and the gas flow rate is weaker than the interaction between the scanning speed and powder flow rate. This is because the gas flow rate has a least significant effect on the wear volume loss. The interaction between the gas flow rate and the scanning speed (see Figure 7e) is also weaker than the interaction between the gas flow rate and the powder flow rate (see Fig 7f).

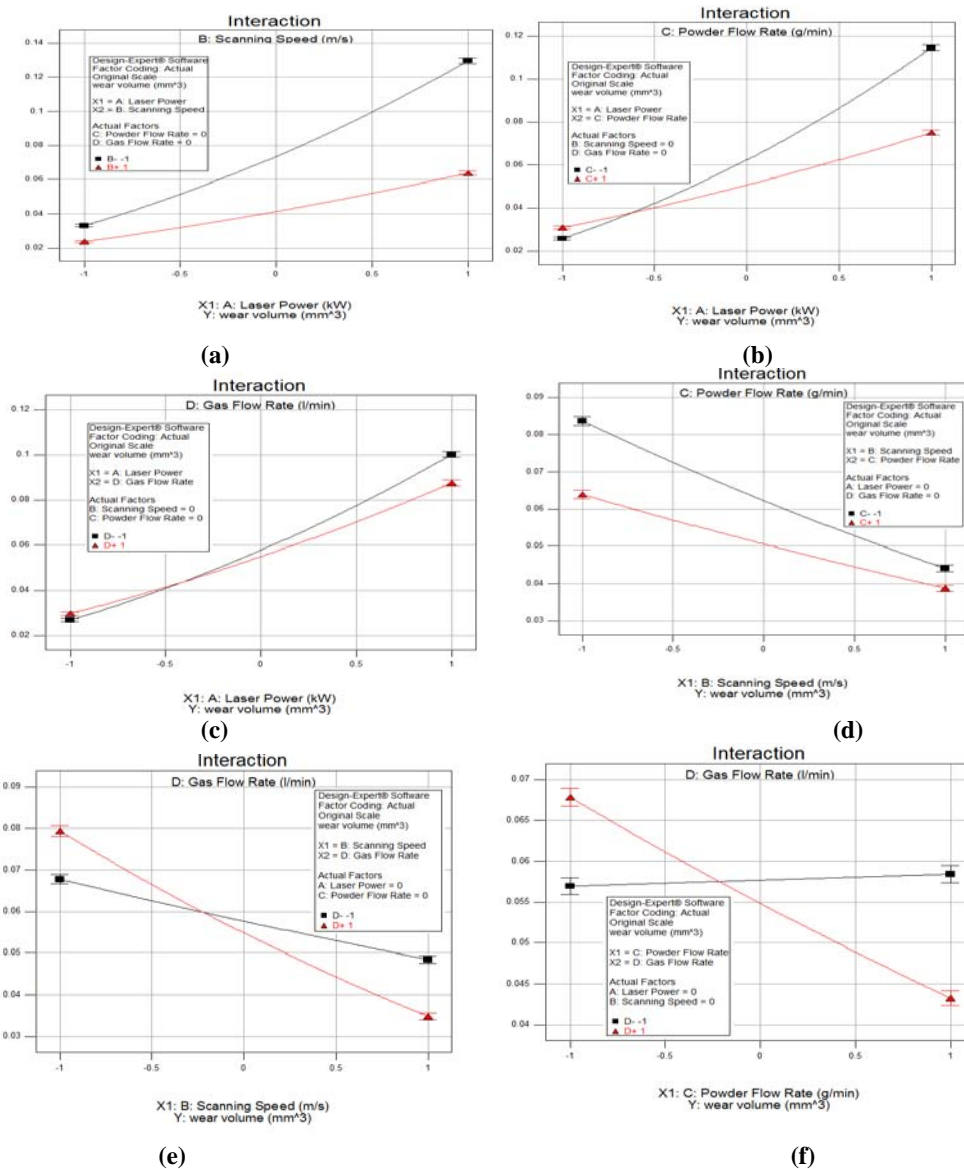


Fig. 7: Interaction plot of: (a) laser power and scanning speed; (b) laser power and powder flow rate

The surface plots shown in Fig. 8 provide further explanation for the various interactions shown in Figure 7. The surface plot of wear volume against laser power and scanning speed shown in Fig. 8a indicates that the wear volume is highest at highest laser power and low scanning speed while the lowest wear volume occurs at low laser power and high scanning speed. This is because at high laser power and low scanning speed, the laser material interaction is very high at low scanning speed that resulted in more melting of the TiC powder. The wear track of samples at high laser power and low scanning speed is shown in Figure 9a and the wear track of sample at low laser power and high scanning speed is shown in Figure 9b. It can be seen from Fig. 9 that the wear action is more severe at high laser power and low scanning speed (see Figure 9a) as compared to at a low laser power and high scanning speed (see Fig. 9b). This as a result of more unmelted TiC powder particles produced at low laser

power and high scanning speed. These unmelted TiC powder particles rub each other as the sliding action continues thereby forming a powdery surface on the sliding surface which as time goes on the ground powder form a protective layer on the sliding surface thereby inhibiting the wear action. There are also unmelted carbide particles at high laser power but they are smaller in size and fewer than those produced at low laser power. They aggravated the wear action by scratching deep on the sliding surfaces thereby aggravating the wear action. Also from the surface plot in Fig. 8a the wear volume is higher at high laser power and high scanning speed compared to at low laser power and low scanning speed. Although they are far less than the wear volume obtained at high laser power and low scanning speed. The wear track of the sample at high laser power and high scanning speed is shown in Figure 9c and that at low laser power and low scanning speed is shown in Figure 9d. At high laser power

and high scanning speed more unmelted TiC powder particles are retained because the laser material interaction time is reduced and the wear resistance is improved. At low laser power and low scanning speed, although the laser material interaction time is high but the laser power is low that helps in retaining more unmelted TiC powder particles. The surface plot, shown in Figure 8b indicates that the highest wear volume occurs at high laser power and low powder flow rate. While the lowest wear volume occur at low laser power and low powder flow rate. The explanation for this behaviour is similar to what happened at high laser power and low scanning speed, in this case,

the low powder flow rate make most of the TiC powder to be completely melted given rise to the effect similar to the one observes in Figure 8a. The surface plot shown in Figure 8c indicates that the highest wear volume occur at high laser power and low gas flow rate. On the other hand, in Figure 8d, the highest wear volume occurs at low scanning speed and low powder flow rate. The highest wear volume is seen in Figure 8e at low powder flow rate and high gas flow rate. Also in Figure 8f the highest wear volume is observed at high gas flow rate and low scanning speed.

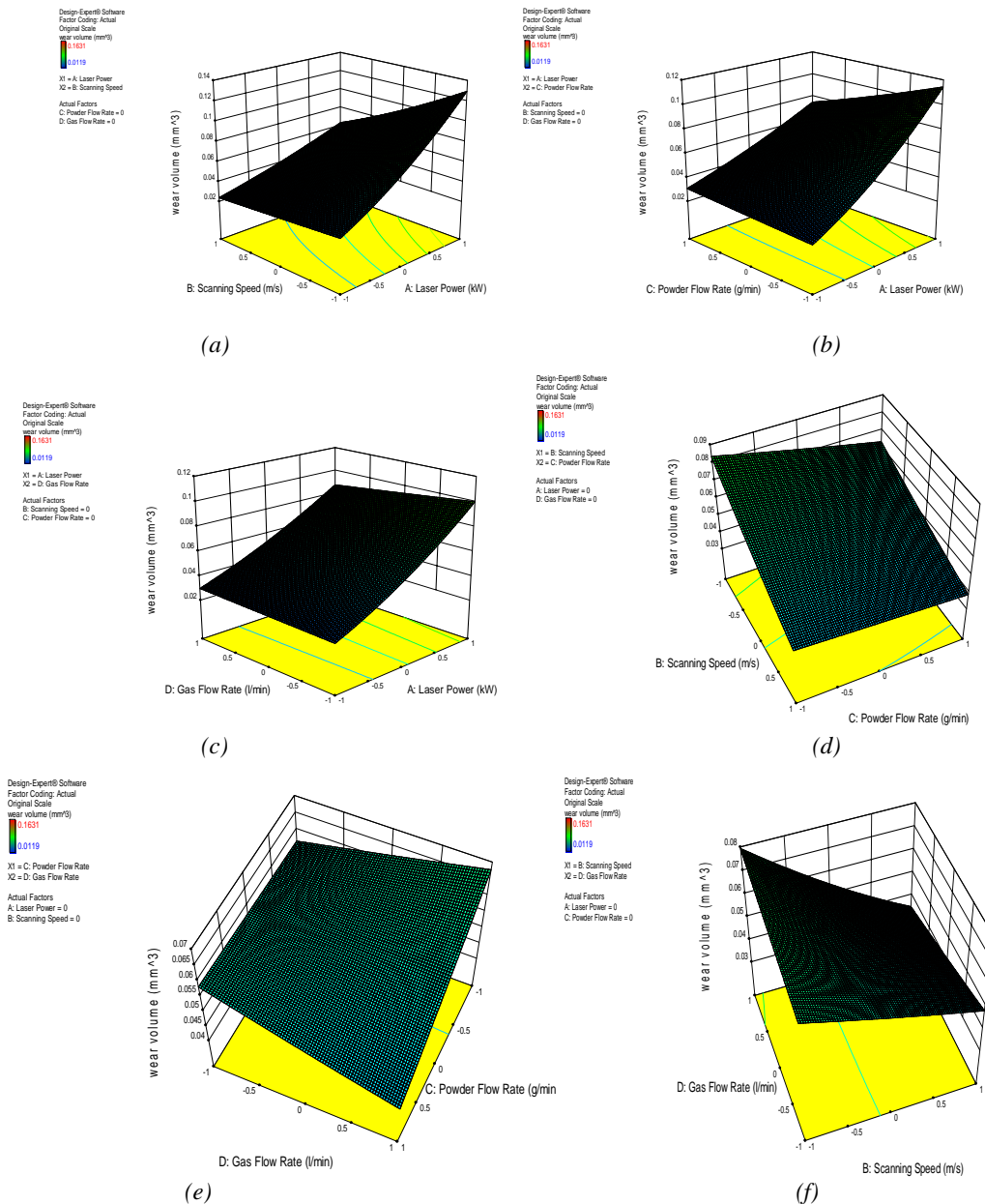


Fig. 8. Surface plot of wear volume against (a) laser power and scanning speed (b) laser power and powder flow rate (c) laser power and gas flow rate (d) Scanning speed and powder flow rate (e) powder flow rate and gas flow rate (f) scanning speed and gas flow rate

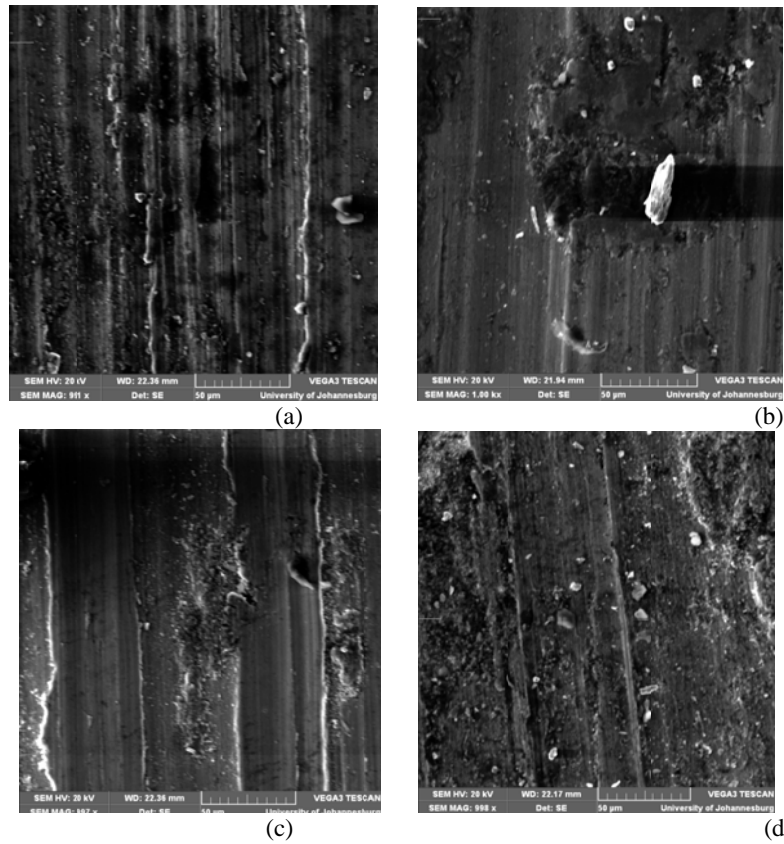


Fig. 9. The micrograph of the wear track of a sample at (a) laser power of 3.2 kW, scanning speed of 0.002 m/s, powder flow rate of 2 g/min and gas flow rate of 2 l/min. (b) laser power of 1.8 kW, scanning speed of 0.006 m/s, powder flow rate of 2 g/min and gas flow rate of 2 l/min (c) laser power of 3.2 kW, scanning speed of 0.006 m/s, powder flow rate of 2 g/min and gas flow rate of 2 l/min. (d) laser power of 1.8 kW, scanning speed of 0.002 m/s, powder flow rate of 2 g/min and gas flow rate of 2 l/min.

To further demonstrate the validity of the developed model, additional experiments were performed at processing parameters different from the ones used in the model development. The results are compared with those predicted by the model.

Model Validation

The validation result is presented in Table 7. The graph of predicted against actual wear volume is shown in Figure 10. It can be seen that the actual experimental data is closed to the predicted values.

Table 7. Validation results for the predicted wear volume and actual wear volume

Number	Laser Power (kW)	Scanning Speed (m/s)	Powder Flow Rate (g/min)	Gas Flow Rate (l/min)	Predicted wear volume (mm ³)	Actual wear volume (mm ³)
1	2.85	0.006	4	4	0.022	0.021
2	1.45	0.006	4	4	0.018	0.019
3	1.8	0.007	4	4	0.011	0.013
4	2.5	0.006	4	3	0.039	0.04
5	2.5	0.004	3	3	0.056	0.055
6	2.85	0.005	3.5	3.5	0.051	0.052
7	1.45	0.003	2.5	2.5	0.046	0.048
8	2.85	0.005	3.5	3.5	0.051	0.05
9	1.8	0.005	2	2	0.017	0.018

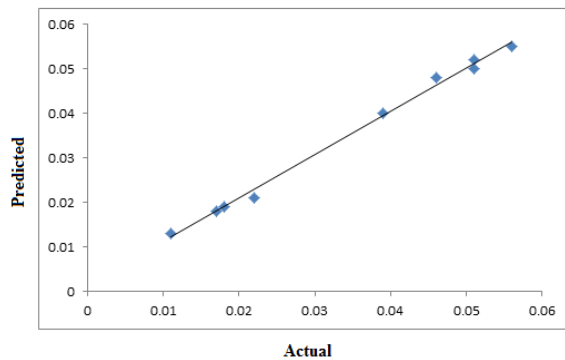


Fig. 10. Plot of predicted versus actual experimental data

4. Conclusion

The effect of laser power, scanning speed, powder flow rate and powder flow rate on wear resistance behaviour of laser deposited TiC/Ti6Al4V composites was investigated in this work. Full factorial design of experiment was employed for the study using Design expert 9, statistical software. A model was developed in this study that is capable of predicting the wear behaviour of laser deposited TiC/Ti6Al4V by varying the processing parameters studied. The model developed was validated by conducting experiment at processing parameters outside the parameters studied and the result was found to be in good agreement with the predicted data. Optimization of the processing parameter was also conducted to minimize the wear volume. There is also good agreement between the predicted optimized parameters and the experimental results. The model can be used to design laser deposited TiC/Ti6Al4V composite for medical and aerospace applications.

Reference

- [1] J. D. Destefani, Metals Handbook ASM International, Materials Park, **2**, 586 (1998).
- [2] M. Peters, J. Kumpfert, C.H. Ward, C. Leyens, Advanced Engineering Materials, **5**, 419 (2003).
- [3] S. Zhang, W.T. Wu, M. C. Wang, H. C. Man, Surface and Coatings Technology, **138**(1), 95 (2001).
- [4] A. R. Machado, J. Wallbank, Management and Engineering Manufacture. **204**(11), 53 (2005).
- [5] O. Momin, S.Z. Shuja, B.S. Yilbas, International Journal of Thermal Sciences **54**, 230 (2012).
- [6] N. M. Tikekar, K.S. R. Chandran, A. Sanders Scripta Materialia, **57**(3), 273 (2007).
- [7] Y. Xing, C. Jiang, J. Hao, Vacuum, **95**, 12 (2013).
- [8] J. Sun, W. P. Tong, L. Zuo, Z. B. Wang, Materials & Design, **47**: 408 (2013).
- [9] Y. S. Tian, C. Z. Chen, S. T. Li, Q. H. Huo, Applied Surface Science, **242**(1-3), 177 (2005).
- [10] J. Ciganovic, J. Stasic, B. Gakovic, M. Momcilovic, D. Milovanovic, M. Bokorov, M. Trtica, Applied Surface Science, **258**(7), 2741 (2012).
- [11] G.X. Luo, G. Q. Wu, Z. Huang, Z.J Ruan, Materials Characterization. **60**(6), 525 (2009).
- [12] J. D. Majumdar, I. Manna, Laser material processing. International Material Reviews **56**(5/6), 341. (2011).
- [13] J. D. Majumdar, I. Manna, (Eds). Laser Assisted Fabrication of Material. Springer Series in Material Science, vol. 161. (2013)
- [14] J. D. Majumdar, Laser gas alloying of Ti-6Al-4V. Physics Procedia, **12**, 472 (2011).
- [15] Y.S. Tian, C.Z. Chen, D.Y. Wang, Q.H. Huo, T.Q. Lei, Applied Surface Science, **250**(1-4), 223 (2005).
- [16] Y.S. Tain, L.X. Chen, C.Z. Chen, Crystal Growth and Design **6**(6), 1509 (2006).
- [17] P. Kadolkar, N.B. Dahotre, Applied Surface Science **199**, 222 (2002).
- [18] A.P.I. Popoola, D.I. Adebisi, Scientific and Essays **6**(29), 6104 (2011).
- [19] A.P.I. Popoola, S.L. Pityana, T. Fedotova, O.M. Popoola, The Journal of the Southern African Institute of Mining and Metallurgy **111**, 335 (2011).
- [20] A.P. I. Popoola, O. F. Ochonogor, M. Abdulwahab, S. Pityana, C. Meacock, J. Optoelectron. Adv. Mater. **14**(11- 12): 991- 997. (2012),
- [21] A. P. I. Popoola, O. F. Ochonogor, M. Abdulwahab, International Journal of Electrochemical Science, **8**, 2449 (2013).
- [22] K. J. Kubiak, W. Pawlak, B. G. Wendler, T. G.Mathia, Wear resistant multilayer nanocomposite WC1-x/C coating on Ti-6Al-4V titanium alloy, 40th Leeds-Lyon Symposium on Tribology &Tribochemistry Forum 2013 September 4-6, 2013, Lyon, France. (2013),
- [23] V. K. Balla, A. Bhat, S. Bose, A. Bandyopadhyay, Journal of the Mechanical Behavior of Biomedical Materials, **6**, 9 (2012)
- [24] R. M. Mahamood, E. T. Akinlabi, M. Shukla, S. Pityana, Materials and Design, **50**, 656 (2013).
- [25] J. Scott, N. Gupta, C. Wember, S. Newsom, T. Wohlers, T. Caffrey, Additive Manufacturing: Status and Opportunity, Science and Technology Policy Institute. (2012),
- [26] X.H. Wu, L. Jing, J. F., Mei, C. Mitchell, P. S. Goodwin, W Voice, Materials and Design, **25**, 137 (2004).
- [27] A. J. Pinkerton, W. Wang, L. Li, Proc. IMechE Part B: J. Engineering Manufacture, **222**, 827 (2008),
- [28] R. M. Mahamood, E. T. Akinlabi, M. Shukla, S. Pityana, Lecture Note in Engineering, WCE 2012, July 4-6,2012, London, United Kingdom, **3**, 1593 (2012).

- [29] R. M. Mahamood, E. T. Akinlabi, M. Shukla, S. Pityana, Characterization of laser deposited Ti6Al4V/TiC composite. *Lasers in Engineering*, Article in Press. (2014).
- [30] K. Makoto, I. Daishi, K. Naoyuki, *Materials* (3) 3939 (2010).
- [31] R. M. Mahamood, E. T. Akinlabi, M. Shukla, S. Pityana, (2013d). Laser metal deposition of Ti6Al4V: A study on the effect of laser power on microstructure and microhardness. *International Multi conference of Engineering and Computer Science (IMECS 2013)*, March 2013.
- [32] S. Sharma, S. Sangal, K. Mondal, *Wear*, **300**(1–2), 82 (2013).
- [33] R. M. Mahamood, E. T. Akinlabi, M. Shukla, S. Pityana (2014). Improving Surface Integrity using Laser Metal Deposition Process. In: Santo, L. and Davim, J. P. Eds. *Surface Engineering Techniques and Applications: Research Advancements*. Pennsylvania (USA): IGI Global, pp. 146-176. DOI: 10.4018/978-1-4666-5141-8.ch005.

*Corresponding author: mahamoodmr2009@gmail.com